IJMAO

International Journal of Mathematical Analysis and Optimization: Theory and Applications
Vol. 2020, No. 1, pp. 669 - 688

Dissipative Nanofluid Slip-Flow and Heat Transfer in a Permeable Stretching Vertical Channel with Internal Heat Generation

H.A. Isede [1*], A. Adeniyan [2]

1*, 2, Department of Mathematics, University of Lagos, Nigeria.
*Corresponding Author email: hisede@unilag.edu.ng

Article Info
Received: 05 April 2019 Revised: 25 April 2020
Accepted: 26 April 2020 Available online: 18 May 2020

Abstract

A comparative investigation is carried out in this paper to study the influence of Alumina and Titanium oxide water based nanofluids abound and flow in a vertical channel whose one of its parallel walls is both permeable and extensible in the presence of thermal dissipation and internal heat source/sink. The governing basic partial differential equations are formulated and reduced to ordinary differential equations by means of existing transformation, thereafter solved using Homotopy Perturbation Method (HPM). Excellent validation of the HPM results has been assessed through comparison with the fourth-fifth-order Runge-Kutta-Fehlberg numerical quadrature by means of tables. For some selected values of various basic flow parameters, tables are contextualized on the skin-friction parameters as well as the surface heat transfer rate. The influence of nanofluid volume fraction, Echert number, viscosity based Reynolds numbers, internal heat generation/absorption, wall mass flux and velocity slip are investigated by means of plotted axial and transverse velocity graphs as well as temperature profiles, and they are found to be highly significant on both velocity and temperature fields. Also, the results indicate that relative differences of the values due to Titanium Oxide from those of the Alumina none-negative in almost all cases with exception of mass flux effect at the wall. In particular, the influence of the nanoparticle volume fraction is to intensify the wall fluid characteristics in both Alumina and Titanium Oxide nanofluids.

Keywords and Phrases Nanofluid; Heat generation; Thermal dissipation; Mass flux; HPM.
MSC2010: 76D99.

1 Introduction

Nanoparticle research is currently an area of intense scientific interest due to a wide variety of potential applications in electronic, biomedical, and optical field. Nanotechnology has received extensive attention in recent years due to enormous applications in food, engineering and transportation, industrial, electronics, nuclear reactors, biomedicine, drug delivery, automobiles and biological

IJMAO

International Journal of Mathematical Analysis and Optimization: Theory and Applications
Vol. 2020, No. 1, pp. 669 - 688

Table 1: Nomenclature of Symbols

Nomenclature		Greek Symbols	
a	Stretching rate.	β	Volumetric coefficient of thermal
C_i	Dimensionless constants, ($i = 1,2,3,4,5,6$)	δ	expansion
C_f	Skin friction	η	Slip parameter
C_p	Specific heat at a constant pressure.	θ	Non-dimensional parameter
Ec	Eckert number.	k	Temperature
f_w	Mass flux parameter.	μ	Thermal conductivity
g	Acceleration due to gravity	υ	Dynamic viscousity
Gr_x	Local Grashof number.	ρ	Kinematic viscosity.
h	Distance between the plates	ϕ	Density.
L	Navier slip factor.		Nanofluid volume.
Nu	Nusselt number (Rate of heat transfer)		.
p	Modified fluid pressure.		
Pr	Prandtl number.		
Q_0	Volumetric heat generation/absorption	**Subscripts**	
Re	Renolds number (viscosity parameter).		
S	Volumetric heat generation/absorption parameter.	f	Base fluid
T	Temperature.	nf	Nanofluid
u, v	Velocity component along x, y axis respectively.	s	Nano-solid-particles
V_w	Wall mass flux.		

sensors. Nanofluids are engineered by suspending nanoparticles with average sizes (1–100 nm). Nanofluids is a term first introduced by Choi [1] and refers to a new class of heat transfer fluids with superior thermal properties. The fluid referred to as a nanofluid is the mixture of the nanoparticles and base fluid having unique physical and chemical properties. The presence of the nanoparticles in the nanofluid is expected to enhance the thermal conductivity and therefore substantially enhance the heat transfer characteristics of the nanofluid. Nanofluidscan be defined as the dilution of nanometer-sized particles (smaller than 100 nm) in a fluid, Das et al. [2].

The nanofluid is modeled as liquid containing nanoparticles, small enough so that the nanoparticles are in thermodynamic and momentum equilibrium as if a single fluid. As such, its behavior as a flowing fluid is modeled after a single component "Navier–Stokes fluid", but the thermophysical properties are obtained by separate calculations, empirical relations or via measurements pertaining to dilute concentration of nano-sized particles embedded in a base liquid.

Tiwari and Das [3] have investigated numerically the behavior of nanofluids inside a two-sided lid-driven differentially heated square cavity to better understand the convective recirculation and flow processes induced by the nanofluid. One of their findings was that the direction of the moving walls affected the fluid flow and heat transfer in the cavity.

Convective flows in vertical channels are significant in the improvement of cooling systems in nuclear reactors, solar cells, heat exchangers, and many other electrical and industrial appliances.

IJMAO

International Journal of Mathematical Analysis and Optimization: Theory and Applications
Vol. 2020, No. 1, pp. 669 - 688

There are many studies of nanofluids in different geometries. On the contrary, the number of studies on nanofluid slip-flow and heat transfer in a stretching vertical channel is limited. Adeniyan and Ajiboye (2016) analyzed an ordinary mixed convective Darcy-Forchimer flow in a channel filled partially with porous substrate of finite thickness attached to one of the channel walls taking into account the influence of permeability, thermal radiation and viscous dissipation.
One recently explored approach for improving the performance of heat transfer in a vertical channel is the work of Mahmoodi and Kandelousi [4], who investigated the kerosene-alumina nanofluid flow and heat transfer in a nozzle of liquid rocket engine. They discovered that using kerosene-alumina nanofluid as fuel of liquid rocket engine can improve the cooling process of its chamber and nozzle walls. Das et al [5] investigated a steady MHD boundary layer flow of an electrically conducting nanofluid over a vertical permeable stretching surface with variable stream conditions. They discovered that increasing thermal radiation parameter with chemical reaction on a nanofluid increases the flow velocity and causes the temperature to decrease.Ellahi [6] studied the magneto-hydrodynamic (MHD) flow of non-Newtonian nanofluid in a pipe. He observed that the MHD parameter reduces the fluid motion and that the velocity profile is larger than the temperature profile even in the presence of variable viscosities. The continuum formulation to developing boundary layer problem, which approximates the entrance region of nanofluid flow in micro channels or tubes was applied by Liu et al [7]. They suggested further molecular dynamics computations of properties of nanofluids, including transport properties, accompanied by careful laboratory experiments on velocity and temperature profiles in order to fully appreciate the potential in the use of nanofluids in heat transfer enhancement. Free convection heat transfer in an enclosure filled with nanofluid was investigated by Sheikholeslami et al. [8]. They discovered that while the Nusselt number is an increasing function of buoyancy ratio number, it is a decreasing function of Lewis number and the angle of turn.Malvandi et al [9] presented a pragmatic approach of boundary layer flow and heat transfer of nanofluid, to reduce the thermal resistance of the plate. Their findings indicated that increasing plate thermal resistance leads to decreases in both heat and concentration rates. Hatami et al. [10] investigated the MHD Jeffery-Hamel nanofluid flow in non-parallel walls. They found that skin friction coefficient is an increasing function of Reynolds number and nanoparticle volume fraction but a decreasing function of Hartmann number. Hayat et al [11] studied the characteristics of boundary layer flow of nanofluid induced by a Riga plate with variable thickness. They noted that velocity distribution shows decreasing behavior for higher values of modified Hartman number, while a higher estimations of Deborah number resulted in the reduction of velocity and momentum boundary layer thickness. The simulation of flow and heat transfer of nanofluid flow between two parallel plates was carried out by Hatami et al. [12]. They showed that in order to reach maximum Nusselt number, copper should be used as nanoparticle. Nanofluid heat transfer enhancement was studied by a number of authors [4,8,10–15,17].
Most real life occurrences are essentially nonlinear and are described by nonlinear equations. Nonlinear differential equations usually arise from mathematical modeling of many physical systems. One exact method that does not require small parameter(s) is the Homotopy perturbation method. Therefore, same as the Homotopy Analysis Method (HAM) and the Differential Transform Method (DTM), the HPM can overcome the restrictions and limitations of perturbation methods. This method continuously deforms the problem to a simple one which is then easy to solve. The homotopy perturbation method is a coupling of the traditional perturbation method and homotopy in topology. It constructs a homotopy $p \in [0,1]$ as a small parameter. The main advantage of this method is that it can be applied directly to nonlinear differential equations without requiring linearization, discretization and therefore, it is not affected by errors associated with discretization. The concept of HPM was first proposed by the Chinese mathematician He [15], who used it to solved some problems with or without small parameters.
In this paper the influence of nanofluid is considered for the boundary layer flow in a vertical channel, in the presence of heat generation/absorption and thermal radiation. The Maxwell (popularly referred to as Tiwari-Das) model is adopted for this study. The basic partial differential equations

IJMAO

International Journal of Mathematical Analysis and Optimization: Theory and Applications
Vol. 2020, No. 1, pp. 669 - 688

are reduced to ordinary differential equations and solved using the Homotopy Perturbation Method (HPM). The velocity and temperature profiles, the skin friction coefficient, and the local Grashof number are plotted for various values of the emergent parameters in the flow, to determine their effects on the flow, and heat transfer characteristics.

2 Mathematical Formulation

The steady flow of a nanofluid between two horizontal parallel plates (Figure 1a,b), is considered in the present study. By virtue of the small nanoparticle size, it can be considered as a homogeneous fluid; hence, it can be described within the framework of the single-fluid approximation, that is one-phase fluid flow. Moreover, the fluid is assumed to be incompressible, and its dynamics is described by the Navier-Stokes equations.
The two opposite parallel walls of the channel is such that the left cold plate at uniform temperature T_0 and located at $y = 0$, is stretching linearly with velocity $u = ax$ and the right hot plate located at $y = h$ is stationary. Any planar point of the cold plate remains unchanged because it is being stretched by two equal and opposite forces. Assumption is also made that there is a slippage on the wall of the cold plate which is proportional to the velocity gradient whilst the hot plate is subjected to moderate uniform thermal heating with temperature T_h. Under fully developed hydrodynamic and thermal flow the constitutive continuity, momentum and energy equations as per the model now follow:

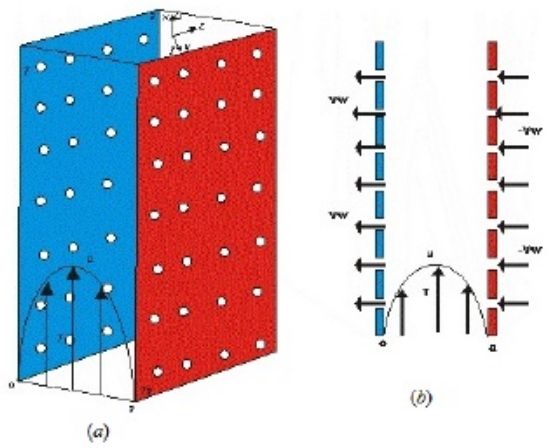

Figure 1: Schematic Diagram of the Physical Model

$$\frac{\partial u}{\partial x} + \frac{\partial v}{\partial y} = 0 \ , \tag{2.1}$$

$$\rho_{nf}\left(u\frac{\partial u}{\partial x} + v\frac{\partial u}{\partial y}\right) = -\frac{\partial p}{\partial x} + \mu_{nf}\left(\frac{\partial^2 u}{\partial x^2} + \frac{\partial^2 u}{\partial y^2}\right) + g(\rho\beta)_{nf}(T - T_0) \ , \tag{2.2}$$

$$\rho_{nf}\left(u\frac{\partial v}{\partial x} + v\frac{\partial v}{\partial y}\right) = -\frac{\partial p}{\partial y} + \mu_{nf}\left(\frac{\partial^2 v}{\partial x^2} + \frac{\partial^2 v}{\partial y^2}\right) \ , \tag{2.3}$$

IJMAO

International Journal of Mathematical Analysis and Optimization: Theory and Applications
Vol. 2020, No. 1, pp. 669 - 688

$$(\rho C_p)_{nf}\left(u\frac{\partial T}{\partial x}+v\frac{\partial T}{\partial y}\right)=k_{nf}\left(\frac{\partial^2 T}{\partial x^2}+\frac{\partial^2 T}{\partial y^2}\right)+Q_0(T-T_0)$$
$$+\mu_{nf}\left(2\left[\left(\frac{\partial u}{\partial x}\right)^2+\left(\frac{\partial v}{\partial y}\right)^2\right]+\left(\frac{\partial v}{\partial x}\right)^2\right). \tag{2.4}$$

Where u and v denote the fluid velocity components along the x and y directions respectively, p is the modified fluid pressure, and T is the fluid temperature. The physical meanings of the other quantities are mentioned in the nomenclature (Table 1).

The boundary conditions are:

$$v=v(x),\quad along\ \ the\ \ y-axis$$
$$u=ax+L\frac{\partial u}{\partial y}\ ,v=v_w\ ,T=T_0\quad at\ y=0$$
$$u=0\ ,v=-v_w\ ,T=T_h\quad at\ y=h\ , \tag{2.5}$$

where $T_0>T_h$, while $a>0$ is the stretching rate, L is the Navier-slip factor, and v_w is the wall mass flux.
Liquid is sucked uniformly over one and injected uniformly over the other, with velocity flux v at the walls. Assuming that the x-axis coincides with the cold plate such that $-\infty<x<\infty$ while y-axis is taken perpendicular to the channel parallel walls where $0\le y\le h$. From continuity equation (1) it follows that everywhere in the channel $v=v(x)\to u=u(y)$ only, and along the y-axis the velocity assumes the form stated.
The properties of the nanofluid are defined as (Choi 1995):

$$\left.\begin{aligned}\mu_{nf}&=\tfrac{\mu_f}{(1-\phi)^{2.5}};\\ \tfrac{k_{nf}}{k_f}&=\tfrac{(k_s+2k_f)-2\phi(k_f-k_s)}{(k_s+2k_f)+\phi(k_f-k_s)}\ ;\\ \beta_{nf}&=\tfrac{(\rho\beta)_{nf}}{\rho_{nf}}=(1-\phi)\beta_f+\phi\beta_s\ ;\\ (\rho C_p)_{nf}&=(1-\phi)(\rho C_p)_f+\phi(\rho C_p)_s\ ;\\ \rho_{nf}&=(1-\phi)\rho_f+\phi\rho_s\end{aligned}\right\} \tag{2.6}$$

It is worthy to mention that the nanoparticles considered here bear spherical shape.The following non-dimensional variables are introduced:

$$\eta=\frac{y}{h}\ ,\ f'(\eta)=\frac{v}{ah}\ ,\ \theta(\eta)=\frac{T-T_0}{T_h-T_0} \tag{2.7}$$

It is seen that the continuity equation (1) is fulfilled identically by (7). The non-dimensional forms of (2) to (4) are as follows:

$$\rho_{nf}\left(a^2xf'^2-a^2xff''\right)=-\frac{\partial p}{\partial x}+\mu_{nf}\left(\frac{ax}{h^2}f'''\right)+g(\rho\beta)_{nf}\left[(T_h-T_0)\theta\right] \tag{2.8}$$

$$\rho_{nf}\left(a^2hff'\right)=-\frac{\partial p}{\partial y}+\mu_{nf}\left(-\frac{a}{h}f''\right) \tag{2.9}$$

IJMAO

International Journal of Mathematical Analysis and Optimization: Theory and Applications
Vol. 2020, No. 1, pp. 669 - 688

$$(\rho C_p)_{nf}\left(-a(T_h-T_0)f\theta'\right)=k_{nf}\left((T_h-T_0)\frac{1}{h^2}\theta'\right)+Q_0(T-T_0)+4\mu_{nf}a^2f'^2 \tag{2.10}$$

Cross differentiating (8) and (9) with respect to y and x respectively, and simplifying, give

$$\rho_{nf}a\frac{h^2}{\mu_{nf}}\left(f'f''-ff'''\right)=f^{iv}+\frac{h^2}{ax\mu_{nf}}g(\rho\beta)_{nf}\left[(T_h-T_0)\theta'\right] \tag{2.11}$$

Using the nanofluid properties in (6) for (10) and (11), the following were obtained respectively,

$$f^{iv}-R_eC_1C_2\left(f'f''-ff'''\right)+C_1C_2C_3Gr_x\theta'=0 \tag{2.12}$$

$$\theta'+P_r\frac{C_5}{C_6}\left(R_ef\theta'+4E_cf'^2\right)+S\frac{C_6}{C_5}\theta=0 \tag{2.13}$$

where

$$\left.\begin{array}{ll} C_1=(1-\phi)^{2.5}\ , & C_2=\left[1+\left(\frac{\rho_s}{\rho_f}-1\right)\phi\right]\ , \\ C_3=\left[1+\left(\frac{\beta_s}{\beta_f}-1\right)\phi\right]\ , & C_4=\left[(1-\phi)+\phi\frac{(\rho C_p)_s}{(\rho C_p)_f}\right]\ , \\ C_5=\left[\left(\frac{k_s}{k_f}+2\right)+\phi\left(1-\frac{k_s}{k_f}\right)\right]\ , & C_6=\left[\left(\frac{k_s}{k_f}+2\right)-2\phi\left(1-\frac{k_s}{k_f}\right)\right]\ . \end{array}\right\} \tag{2.14}$$

and

$$\left.\begin{array}{lll} R_e=\frac{h^2a}{\nu_f}\ , & Gr_x=\frac{g(\rho\beta)_f(T_h-T_0)h^2}{u_w\mu_f}\ , & u_w=ax\ , \\ P_r=\frac{\nu_f(\rho C_p)_f}{k_f}\ , & S=\frac{Q_0h^2}{k_f}\ , & E_c=\frac{\mu_fh^2a^2}{k_f(T_h-T_0)}\ . \end{array}\right\} \tag{2.15}$$

Where R_e is the Renolds number (viscosity parameter), Gr_x is the local Grashof number, ν is the kinematic viscosity, P_r is the Prandtl number, S is the volumetric heat generation/absorption parameter, and E_c is the Eckert number, β is the volumetric coefficient of thermal expansion,k is the thermal conductivity.
The boundary conditions become

$$\left.\begin{array}{lll} f=-f_w\ , & f'=1+\delta f''\ , & \theta=1\ :\ \eta=0 \\ f=f_w\ , & f'=0\ , & \theta=0\ :\ \eta=1\ . \end{array}\right\} \tag{2.16}$$

Here, f_w is the mass flux parameter and δ is the slip parameter.
The local skin friction coefficient C_{fx} along the stretching wall, which is the physical property of interest in this problem, is defined as

$$C_{fx}=\frac{\tau_w}{\rho_fu_w^2} \tag{2.17}$$

where $\tau_w=\mu_{nf}\left.\frac{\partial u}{\partial y}\right|_{y=0}$ is the wall shear stress, and

$$C_{fr}=C_{fx}Re_x=\frac{1}{C_1}f''(0) \tag{2.18}$$

IJMAO

International Journal of Mathematical Analysis and Optimization: Theory and Applications
Vol. 2020, No. 1, pp. 669 - 688

is the reduced local skin friction coefficient at the stretching wall, with $Re_x = \frac{U_w h}{\nu_f}$ is the local Reynolds number (stretching wall velocity based Reynolds number).
Another physical quantity of importance is the heat transfer rate or Nusselt number at the cold plate. It is defined as

$$Nu_x = \frac{xq_w}{k_f(T_0 - T_h)} \tag{2.19}$$

where $q_w = -k_{nf} \left.\frac{\partial T}{\partial y}\right|_{y=0}$, and

$$Nur = Nu_x R_e Re_x^{-1} = -\frac{k_{nf}}{k_f}\theta'(0) = -\frac{C_6}{C_5}\theta'(0) \tag{2.20}$$

is the reduced Nusselt number.
Table 2 below indicates the thermophysical properties of water, Aluminium Oxide and Titanium Oxide, at the reference temperature [17].

Table 2 : Thermophysical properties of water, Alumina and Titanium Oxide

Physical properties	Base Fluid (Pure Water)	Nanoparticles (Alumina)	Nanoparticles (Titanium Oxide)
$C_p(J/kgK)$	4179	765	682.2
$\rho(kg/m^3)$	997.1	3970	4250
$k(W/mK)$	0.613	40	8.9538
$\beta(K^{-1})$	21×10^{-5}	0.85×10^{-5}	0.90×10^{-5}

3 Homotopy Perturbation Method

The operations of the Homotopy Perturbation method as it relates to the present problem to solve (12),(13) and (16) are given here.
The two variables of interest are defined in (21) and (22) as:

$$f(\eta) = \sum_{i=0}^{\infty} p^i f_i \ , \tag{3.1}$$

$$\theta(\eta) = \sum_{i=0}^{\infty} p^i \theta_i \ . \tag{3.2}$$

In the series (21) and (22), the highest value for i is chosen depending on the desired accuracy. The present study stopped at $i = 2$.

IJMAO

International Journal of Mathematical Analysis and Optimization: Theory and Applications
Vol. 2020, No. 1, pp. 669 - 688

The homotopy perturbation method [16] is given as

$$(1-p)(\textit{highest order derivative in the equation}) + p(\textit{whole equation}) = 0 \tag{3.3}$$

where the "whole equation" in (23) refers to the problem to be solved, i.e. (12) and (13), these become

$$(1-p)f^{iv} + p\left[f^{iv} - R_eC_1C_2\left(f'f'' - ff'''\right) + Gr_xC_1C_2C_3\theta'\right] = 0\ , \tag{3.4}$$

$$(1-p)\theta'' + p\left[\theta'' + Pr\frac{C_5}{C_6}\left(R_ef\theta' + 4E_cf'^2\right) + S\frac{C_4}{C_5}\theta\right] = 0\ . \tag{3.5}$$

Expansions of (24) and (25) yield

$$f^{iv} - pR_eC_1C_2\left(f'f'' - ff'''\right) + pGr_xC_1C_2C_3\theta' = 0\ , \tag{3.6}$$

$$\theta'' + pPr\frac{C_5}{C_6}\left(R_ef\theta' + 4E_cf'^2\right) + pS\frac{C_4}{C_5}\theta = 0\ . \tag{3.7}$$

Substituting for f and θ and their derivatives in (26) and (27), using (21) and (22), give

$$\begin{aligned} &f_0^{iv} + pf_1^{iv} + p^2f_2^{iv} - pR_eC_1C_2\left[(f_0' + pf_1' + p^2f_2')\right. \\ &\quad -\left((f_0 + pf_1 + p^2f_2)(f_0''' + pf_1''' + p^2f_2''')\right] \\ &\quad \left. + pGr_xC_1C_2C_3(\theta_0' + p\theta_1' + p^2\theta_2') = 0\ , \right. \end{aligned} \tag{3.8}$$

$$\begin{aligned} &\theta_0'' + p\theta_1'' + p^2\theta_2'' + pPr\frac{C_5}{C_6}\left[R_e(f_0 + pf_1 + p^2f_2)(\theta_0' + p\theta_1' + p^2\theta_2')\right. \\ &\left. +4E_c(f_0' + pf_1' + p^2f_2')^2\right] + pS\frac{C_4}{C_5}(\theta_0 + p\theta_1 + p^2\theta_2) = 0\ . \end{aligned} \tag{3.9}$$

The associated boundary conditions are similarly obtained using (21) and (22) in (16), and equating coefficients. They therefore become,
for $\eta = 0$:

$$\left.\begin{array}{lll} f_0(0) = -f_w\ , & f_1(0) = 0\ , & f_2(0) = 0 \\ f_0'(0) = 1 + \delta f_0''(0)\ , & f_1'(0) = 0\ , & f_2'(0) = 0 \\ \theta_0(0) = 1\ , & \theta_1(0) = 0\ , & \theta_2(0) = 0\ . \end{array}\right\}\ , \tag{3.10}$$

for $\eta = 1$:

$$\left.\begin{array}{lll} f_0(1) = f_w\ , & f_1(1) = 0\ , & f_2(1) = 0 \\ f_0'(1) = 0\ , & f_1'(1) = 0\ , & f_2'(1) = 0 \\ \theta_0(1) = 0\ , & \theta_1(1) = 0\ , & \theta_2(1) = 0\ . \end{array}\right\}\ . \tag{3.11}$$

The solution for (28) and (29) are obtained by solving the various coefficients of p (that is p^0, p, p^2) one after the other, first in (28), and then in (29).

$$p^0: \quad f_0^{iv} = 0\ .$$

IJMAO

International Journal of Mathematical Analysis and Optimization: Theory and Applications
Vol. 2020, No. 1, pp. 669 - 688

Integrate successively with respect to η to obtain the following

$$\int f_0^{iv} = \int 0 \quad \rightarrow f_0''' = a \;\; ; \;\; \int f_0''' = \int a \quad \rightarrow \;\; f_0''(\eta) = a\eta + b$$

$$\int f_0'' = \int a\eta + b \quad \rightarrow \;\; f_0'(\eta) = \frac{a}{2}\eta^2 + b\eta + c \;\; ;$$

$$\int f_0' = \int \frac{a}{2}\eta^2 + b\eta + c \quad \rightarrow \;\; f_0(\eta) = \frac{a}{6}\eta^3 + \frac{b}{2}\eta^2 + c\eta + d \; .$$

Now the boundary conditions of (30) and (31) are used to obtain the values of a, b, c, and d as

$$a = 3.28888 \;\; , \;\; b = -2.59259 \;\; , \;\; c = 0.94815 \;\; , \;\; d = -f_w = -0.1 \; .$$

Therefore

$$f_0(\eta) = \frac{3.28888}{6}\eta^3 + \frac{-2.59259}{2}\eta^2 + 0.94815\eta - 0.1 \; ,$$

that is

$$f_0(\eta) = 0.54815\eta^3 - 1.2963\eta^2 + 0.94815\eta - 0.1 \; . \tag{3.12}$$

The coefficients of p^0 are also solved in (29) as follows

$$p^0 : \;\; \theta_0'' = 0 \; .$$

Integrate successively with respect to η to obtain the following

$$\int \theta_0'' = \int 0 \quad \rightarrow \theta_0' = a_1 \;\; ; \;\; \int \theta_0' = \int a_1 \quad \rightarrow \quad \theta_0(\eta) = a_1\eta + b_1$$

and the boundary condition of (30) and (31) are used to obtain the values of a_1 and b_1 as

$$a_1 = -1 \;\; , \;\; b_1 = 1 \; ,$$

therefore

$$\theta_0(\eta) = -\eta + 1 \; . \tag{3.13}$$

The coefficients of p, p^2 are similarly solved for $f_1(\eta), f_2(\eta), \theta_1(\eta)$, and $\theta_2(\eta)$ using (28) and (29) until equations such as (32) and (33) are obtained for the velocity (f) and tempearture (θ) respectively. The values for f and θ are finally obtained by adding the the respective subscripted values obtained.

$$f = f_0 + f_1 + f_2 \;\; ; \;\; \theta = \theta_0 + \theta_1 + \theta_2 \tag{3.14}$$

4 Results and Discussion

The thermophysical parameters of real life applications considered in this study for both Alumina and Titanium Oxide include: nanoparticle volume fraction, Reynolds number (R_e), Eckert number (E_c), max flux suction/injection (f_w), Prandtl number (Pr), volumetric heat generation/absorption (S), and local Grashof number (Gr_x). The influence of these parameters on the velocity profile, the temperature profile, the skin friction (C_f), and the Nusselt number (Nu) were investigated graphically and tabularly.

IJMAO

International Journal of Mathematical Analysis and Optimization: Theory and Applications
Vol. 2020, No. 1, pp. 669 - 688

4.1 HPM/Numerical Results

Here, attention is focused on envisioning and analyses in terms of the effects of basic flow parameters on the skin friction alongside the heat transfer rates at the wall surface of the channel with the aids of tables. The HPM results presented are of order p^2.
Table 3a unveils the influence of various basic flow parameters on the skin friction coefficient and the Nusselt number for Alumina nanofluid, using both the HPM and numerical results. As can be seen, increment in the Rayleigh viscous parameter, R_e signifies amplification in not only the reduced skin friction coefficient, but also the reduced Nusselt number. Similar result is observed due to increment in Eckert number, E_c. However, increment in max flux suction/injection leads to increment in both wall parameters for the two nanoparticles under investigation, with the exception of the result of the Nusselt number (this is unexpected but it is script value). The influence of the Prandtl number, Pr is to dampen skin friction and magnify the Nusselt number. The reduced skin friction increases with increments in the internal heat generation but a contrast is the case for the Nusselt number. Influence of the nanoparticle volume fraction is to intensify the wall fluid characteristics (reduced skin friction coefficient and reduced wall rate of heat transfer).

Table 3a : Computations showing results for variations of each dimensionless parameter for Alumina.

								Alumina			
R_e	Gr_x	δ	f_w	P_r	S	E_c	ϕ	Numerical		HPM	
1	**2**	**0.02**	**0.1**	**5**	**0.1**	**0.01**	**0.02**	$-\frac{1}{C_1}f''(0)$	$-\frac{C_2}{C_1}\theta'(0)$	$-\frac{1}{C_1}f''(0)$	$-\frac{C_2}{C_1}\theta'(0)$
1								2.618906	1.176913	2.615376	1.200813
5								2.82768	1.63052	2.81673	1.62918
7								2.92982	1.77036	2.9492	1.77125
1	1							2.70258	1.17343	2.7056	1.13535
	20							1.08844	1.23925	1.13251	1.35066
	40							0.66115	1.30717	0.65628	1.26449
	2	0.01						2.61891	1.17691	2.60722	1.19565
		0.02						2.61891	1.17691	2.60627	1.18257
		0.03						2.72778	1.07432	2.74892	1.11132
		0.02	0.2					1.43925	1.05987	1.42761	1.13559
			0					3.80181	1.29313	3.82142	1.32708
			-0.2					6.17781	1.50835	6.37977	-0.1037
			0.1	1				2.62592	1.08172	2.62606	1.0815
				10				2.61113	1.29323	2.56292	1.34655
				20				2.59911	1.50371	2.54057	1.45438
				5	20			2.62008	1.07813	2.61733	1.02442
					0			2.6189	1.1774	2.59205	1.36054
					-20			2.61783	1.27301	2.59173	1.44905
					0.1	0.01		2.61891	1.17691	2.59205	1.36008
						0.05		2.61852	1.08651	2.58151	1.35678
						0.1		2.61805	0.97344	2.56249	1.34513
						0.01	0.02	2.61891	1.17691	2.60627	1.18257
							0.6	25.5935	5.13941	25.5928	5.15403
							0.7	52.6104	7.16317	52.6102	7.17102

IJMAO

International Journal of Mathematical Analysis and Optimization: Theory and Applications
Vol. 2020, No. 1, pp. 669 - 688

Table 3b addresses the influence of various flow fluid parameters on reduced skin friction coefficient and reduced Nusselt number as per Titanium Oxide.
Both the skin friction coefficient and the Nusselt number intensify in magnitude as the Reynolds viscous parameter increases. Both reduced skin friction and reduced Nusselt number intensify in values as the suction/injection parameter increases. The result of increasing the Prandtl number for the Titanium Oxide is similar to that of Alumina, already discussed. Increment in the suction/injection is to magnify both reduced skin friction coefficient and the reduced Nusselt number. Increment in the Eckert number diminishes the reduced skin friction coefficient as well as the reduced Nusselt number of the Titanium Oxide nanofluid.

Table 3b: Computations showing results for variations of each dimensionless parameter for Titanium Oxide.

								Titanium Oxide			
								Numerical		HPM	
R_e	Gr_x	δ	f_w	P_r	S	E_c	ϕ	$-\frac{1}{C_1}f''(0)$	$-\frac{C_3}{C_2}\theta'(0)$	$-\frac{1}{C_1}f''(0)$	$-\frac{C_3}{C_2}\theta'(0)$
1	**2**	**0.02**	**0.1**	**5**	**0.1**	**0.01**	**0.02**				
5								2.618281	1.176415	2.630778	1.094651
7								2.828039	1.633059	2.874423	1.629183
1	1							2.930682	1.772961	2.886001	1.771251
	20							2.70242	1.172878	2.688966	1.350131
	40							1.078958	1.239638	1.13257	1.065589
	2	0.01						0.681267	1.308514	0.776904	1.150299
		0.02						2.618281	1.176415	2.706914	1.18139
		0.03						2.618281	1.176415	2.630778	1.094651
		0.02	0.2					2.727766	1.078627	2.772737	1.071802
			0					2.618281	1.176415	2.630778	1.094651
			-0.2					4.98767	1.406527	4.911296	1.424307
			0.1	1				6.177554	1.51065	6.181318	1.511894
				10				2.625393	1.08033	2.625532	1.071484
				20				2.610407	1.293774	2.624519	1.161676
				5	20			2.598279	1.505778	2.59751	1.494357
					0			2.62222	0.865576	2.640863	0.805557
					-20			2.61529	1.457529	2.605741	1.472052
					0.1	0.01		2.614477	1.544402	2.612826	1.676714
						0.05		2.618281	1.176415	2.630778	1.094651
						0.1		2.617895	1.085281	2.626	1.100668
						0.01	0.02	2.618281	1.167012	2.60595	1.168663
							0.6	25.59062	4.003258	25.58903	4.026686
							0.7	52.61011	5.130742	52.60948	5.145799

The results in Table 4 indicate that relative differences of the values due to Titanium Oxide from those of the Alumina are non-negative in almost all cases with the exception of mass flux effect at the wall.

IJMAO

International Journal of Mathematical Analysis and Optimization: Theory and Applications
Vol. 2020, No. 1, pp. 669 - 688

Table 4: Relative differences of results for variations of each dimensionless parameter for Alumina and Titanium Oxide.

R_e	Gr_x	δ	f_w	P_r	S	E_c	ϕ	Cfr		Relative Difference	Nur		Relative Difference
1	2	0.02	0.1	5	0.1	0.01	0.02	Alumina	Titanium Oxide		Alumina	Titanium Oxide	
1								2.615376	2.630778	0.015402	1.200813	1.094651	0.106162
5								2.81673	2.874423	0.057691	1.62918	1.629183	0
7								2.9492	2.886001	-0.0632	1.77125	1.771251	0
1	1							2.7056	2.688966	-0.01664	1.13535	1.350131	-0.21478
	20							1.13251	1.13257	5.7E-05	1.35066	1.065589	0.285071
	40							0.65628	0.776904	0.120623	1.26449	1.150299	0.114191
	2	0.01						2.60722	2.706914	0.099693	1.19565	1.18139	0.014257
		0.02						2.60627	2.630778	0.024513	1.18257	1.094651	0.087915
		0.03						2.74892	2.772737	0.02382	1.11132	1.071802	0.039519
		0.02	0.2					1.42761	1.434164	0.006556	1.13559	1.054072	0.081518
			0					3.82142	3.819914	-0.0015	1.32708	1.33045	-0.00337
			-0.2					6.37977	6.181318	-0.19846	-0.1037	1.511894	-1.61562
			0.1	1				2.62606	2.625532	-0.00053	1.0815	1.071484	0.010017
				10				2.56292	2.624519	0.061595	1.34655	1.161676	0.184871
				20				2.54057	2.59751	0.05694	1.45438	1.494357	-0.03998
				5	20			2.61733	2.647424	0.030094	1.02442	0.756435	0.267982
					0			2.59205	2.63081	0.038761	1.36054	1.096261	0.264278
					-20			2.59173	2.612826	0.021097	1.44905	1.676714	-0.22767
					0.1	0.01		2.59205	2.630778	0.038727	1.36008	1.094651	0.265431
						0.05		2.58151	2.626	0.044489	1.35678	1.100668	0.256115
						0.1		2.56249	2.619142	0.056657	1.34513	1.0076	0.337529
						0.01	0.02	2.60627	2.60595	0.000315	1.18257	1.168663	0.013908
							0.6	25.5928	25.58903	0.00373	5.15403	4.026686	1.127343
							0.7	52.6102	52.60948	0.00069	7.17102	5.145799	2.025225

4.2 4.2 Graphical Results

4.2.1 Effect of parameter variation on velocity and temperature profiles

The following figures show the impact of some of the parameter variations on the temperature and velocity profiles.
Figure 2 shows the effect of Local Grashof number (Gr_x) on transverse velocity. $R_e = 1$, $\delta = 0.02$, $f_w = 0.1$, $Pr = 5$, $S = 0.1$, $E_c = 0.01$, $\phi = 0.02$.

IJMAO

International Journal of Mathematical Analysis and Optimization: Theory and Applications
Vol. 2020, No. 1, pp. 669 - 688

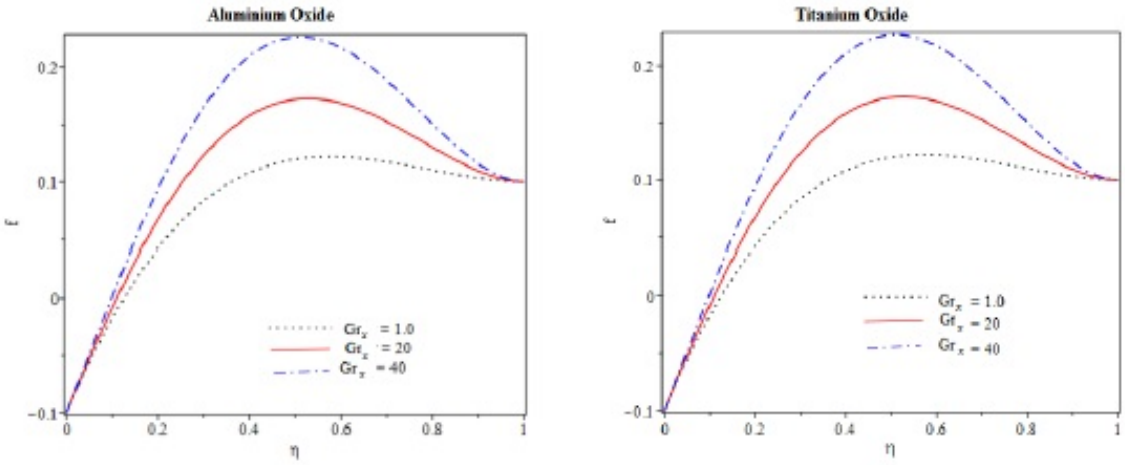

Figure 2: Effect of Local Grashof Number (Gr_x) on Transverse Velocity.

Figure 3 shows the effect of Local Grashof number (Gr_x) on temperature profile. $R_e = 1$, $\delta = 0.02$, $f_w = 0.1$, $Pr = 5$, $S = 0.1$, $E_c = 0.01$, $\phi = 0.02$.

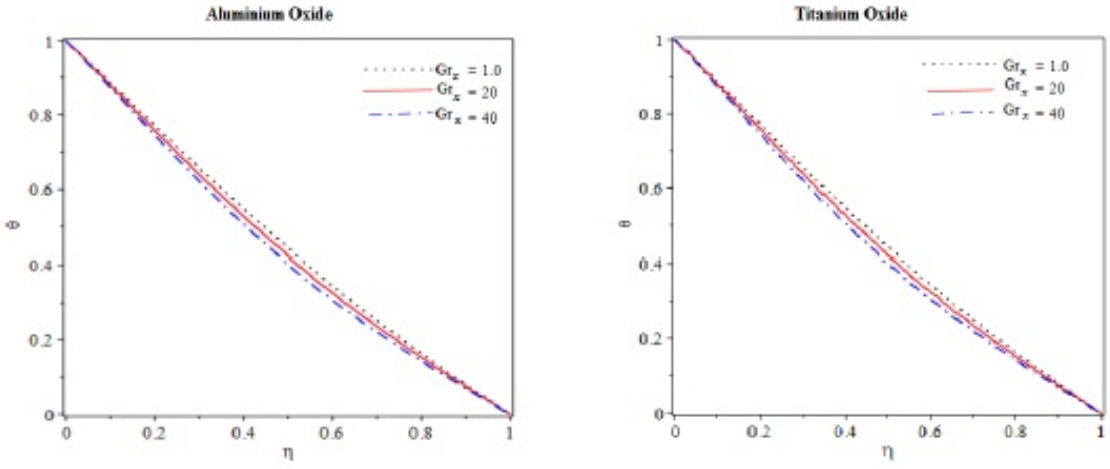

Figure 3: Effect of Local Grashof Number (Gr_x) on Temperature Profile.

Figure 4 shows the effect of Viscosity Parameter (R_e) on temperature profile. $S = 0.1$, $\delta = 0.02$, $f_w = 0.1$, $Pr = 5$, $S = 0.1$, $E_c = 0.01$, $\phi = 0.02$.

IJMAO

International Journal of Mathematical Analysis and Optimization: Theory and Applications
Vol. 2020, No. 1, pp. 669 - 688

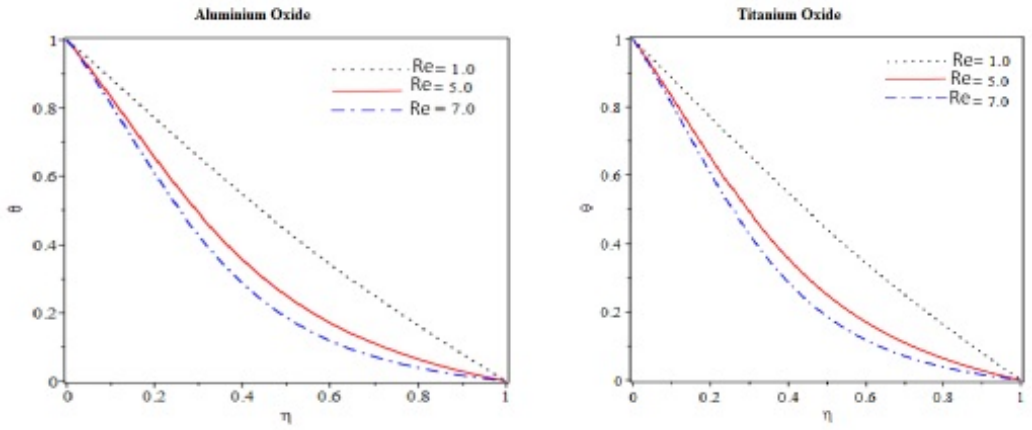

Figure 4: Effect of Viscosity Parameter (R_e) on Temperature.

Figure 5 shows theeffect of Viscosity Parameter (R_e) on transverse velocity profile. $Pr = 5$, Gr_x=2, $\delta = 0.02$, $f_w = 0.1$, $S = 0.1$, $E_c = 0.01$, $\phi = 0.02$.

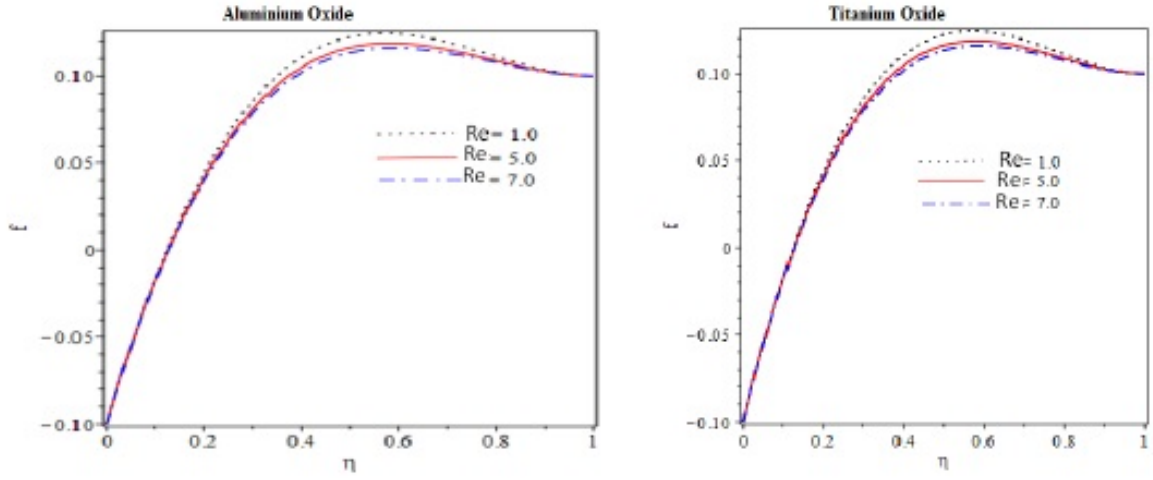

Figure 5: Effect of Viscosity Parameter (R_e) on Transverse Velocity.

Figure 6 shows the effect of Viscosity Parameter (R_e) on axial velocity profile. $Pr = 5$, Gr_x=2, $\delta = 0.02$, $f_w = 0.1$, $S = 0.1$, $E_c = 0.01$, $\phi = 0.02$.

IJMAO

International Journal of Mathematical Analysis and Optimization: Theory and Applications
Vol. 2020, No. 1, pp. 669 - 688

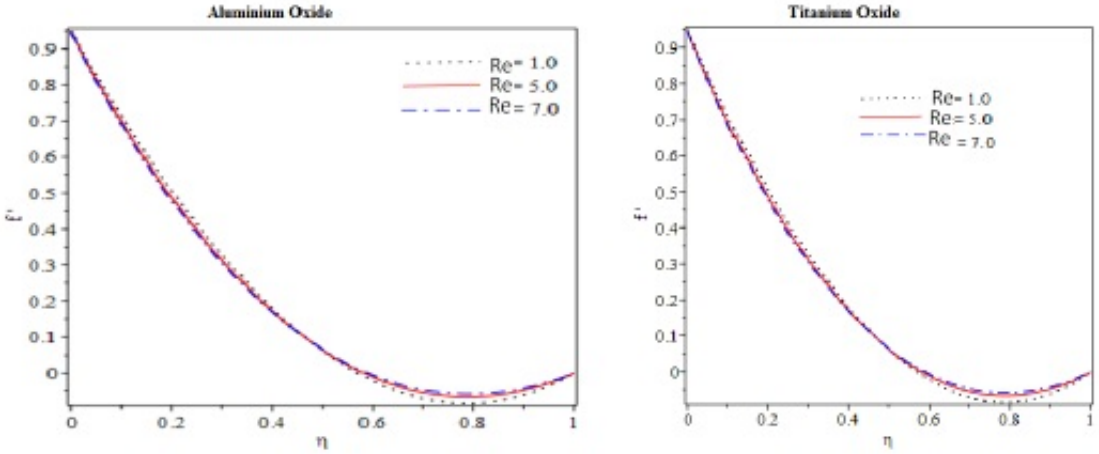

Figure 6: Effect of Viscosity Parameter (R_e) on Axial Velocity.

Figure 7 shows the effect of Local Grashof Number (Gr_x) on axial velocity profile. $R_e = 1$, $\delta = 0.02$, $f_w = 0.1$, $S = 0.1$, $E_c = 0.01$, $Pr = 5$, $\phi = 0.02$.

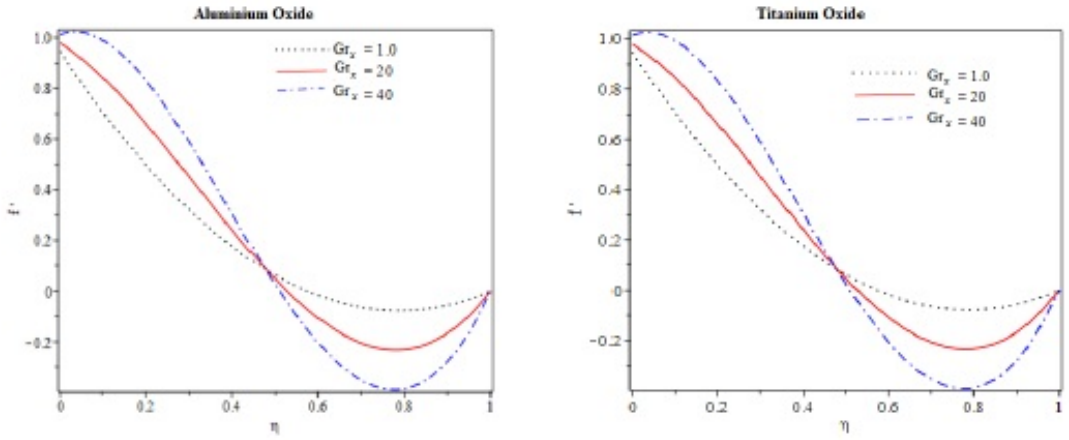

Figure 7: Effect of Local Grashof Number (Gr_x) on Axial Velocity Profile.

Figure 8 shows the effect of Prandtl Number (Pr) on temperature profile. $R_e = 1$, Gr_x=2, $\delta = 0.02$, $f_w = 0.1$, $S = 0.1$, $E_c = 0.01$, $\phi = 0.02$.

IJMAO

International Journal of Mathematical Analysis and Optimization: Theory and Applications
Vol. 2020, No. 1, pp. 669 - 688

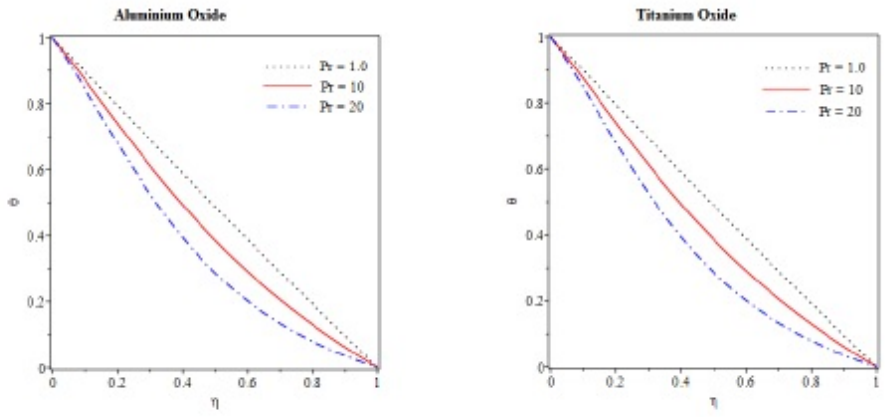

Figure 8: Effect of Prandtl Number (Pr) on Temperature.

Figure 9 shows the effect of Max Flux parameter (f_w) on transverse velocity profile. $R_e = 1$, Gr_x=2, $\delta = 0.02$, $Pr = 5$, $S = 0.1$, $E_c = 0.01$, $\phi = 0.02$.

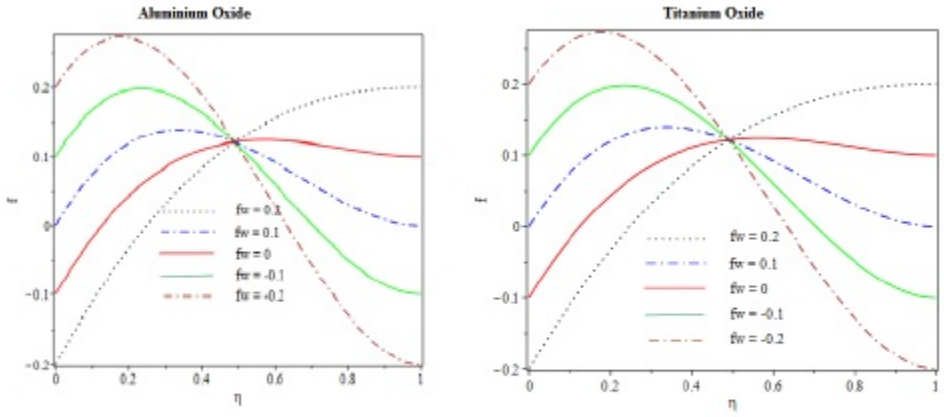

Figure 9: Effects of Max Flux parameter (f_w) on Transverse Velocity.

Figure 10 shows the effect of Max Flux parameter (f_w) on axial velocity profile. $R_e = 1$, Gr_x=2, $\delta = 0.02$, $Pr = 5$, $S = 0.1$, $E_c = 0.01$, $\phi = 0.02$.

IJMAO

International Journal of Mathematical Analysis and Optimization: Theory and Applications
Vol. 2020, No. 1, pp. 669 - 688

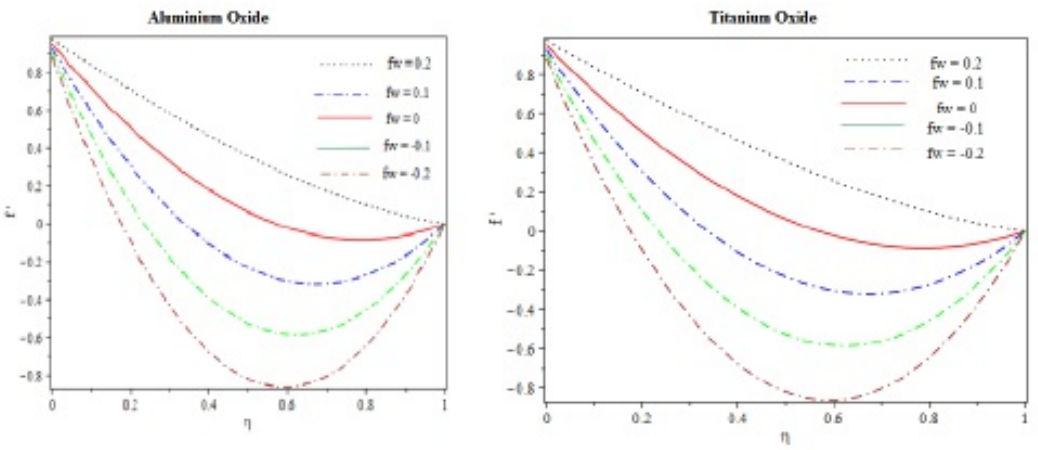

Figure 10: Effects of Max Flux parameter (f_w) on Axial Velocity Profile.

Figure 11 shows the effect of Max Flux parameter (f_w) on temperature profile. $R_e = 1$, Gr_x=2, $\delta = 0.02$, $Pr = 5$, $S = 0.1$, $E_c = 0.01$, $\phi = 0.02$.

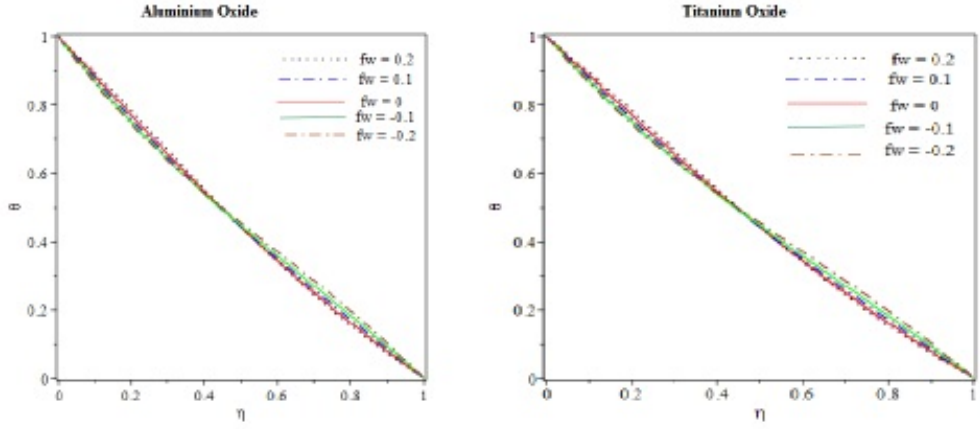

Figure 11: Effects of Max Flux parameter (f_w) on Temperature.

From Figures 2a-11b, the influence of variations of the values of the thermophysical parameters on the profiles is exposed. It is noted that increasing the values of the local Grashof number increases the velocity profiles (Figure 2), but reduces the temperature profiles (Figure 3), of both the Alumina nanofluid (a), and Titanium Oxide nanofluid (b). An increase Grx increases the transverse velocity but decreases the temperature of both nanofluids. This increment of Gr_x also enhances the axial velocity (Figure 7), for both nanofluids.
It is also seen that increasing the values of the Reynold number decreases the temperature profiles (Figures 4), and the velocity profiles (Figures 5), of both the Alumina nanofluid (a), and Titanium

Oxide nanofluid (b). An increase Re reduces the temperature and the transverse velocity of both nanofluids. This increment of Re also reduces the axial velocity (Figure 6), for both nanofluids. From Figure 8, an increase in the values of the Prandtl number decreases the temperature profiles of both the Alumina nanofluid (a), and Titanium Oxide nanofluid (b). An increase Pr reduces the temperature of both nanofluids.
It is noted in Figure 9 that the smaller the negative values of the max flux parameter (f_w) the higher the velocity profile, while the bigger the positive values the lower the velocity profile at the lower half of the wall. The reverse is the case at the upper half of the wall. This is observed for both the Alumina and Titanium Oxide nanofluids.
In Figure 10, an increase in the positive values of the max flux parameter (fw) increases the axial velocity profiles while a decrease in the negative values of the max flux parameter (fw) reduces the axial velocity profiles of both the Alumina nanofluid (a), and Titanium Oxide nanofluid (b).

5 Conclusion

A comparative investigation has been carried out to study the influence of Alumina and Titanium oxide water based nanofluids flows in a vertical channel with two parallel walls both permeable and extensible, in the presence of thermal dissipation and internal heat source/sink.
The results reveal the following.
1. An increase in the Reynolds viscous parameter, R_e signifies increases in both the reduced skin friction coefficient and the reduced Nusselt number of the Alumina nanofluid. This outcome is also the case for the Titanium Oxide nanofluid.
2. An increase in the Eckert number, E_c brings about increases in both the reduced skin friction coefficient and the reduced Nusselt number of the Alumina nanofluid. But the converse is the case with the Titanium Oxide nanofluid, where the reduced skin friction coefficient and the reduced Nusselt number are both diminished.
3. As for the max flux suction/injection, its increase leads to increments in both wall parameters for the two nanoparticles under investigation, with the exception of the result of the Nusselt number for Alumina (this is unexpected, but it is script value).
4. The influence of the Prandtl number, Pr is to dampen the skin friction and magnify the Nusselt number for the Alumina nanofluid. The same is observed for the Titanium Oxide nanofluid, where an increment in the Prandtl number also results in a reduction in the skin friction but an increase in the Nusselt number.
5. Influence of the nanoparticle volume fraction is to intensify the wall fluid characteristics (reduced skin friction coefficient and reduced wall rate of heat transfer), when it is increase. This is the result for both the Alumina and Titanium Oxide nanofluids.
6. The reduced skin friction increases with increment in internal heat generation but contrast is the case for the Nusselt number.

Acknowledgement

The authors of this paper appreciate the efforts of the reviewers of the paper in taking out time to read through and make observations that has enriched this study. Your contributions have further advanced the annals of research. Thank you.

References

[1] Choi, S.U.S. EnhancingThermal Conductivity of Fluids with Nanoparticles. *The proceedings of the 1995 ASME int. mech. eng. congress and exposition*, vol. 66, pp. 99-105, (1995).

[2] Das, S.K., Choi, S.U.S., Yu, W., Pradeep, T. Nanofluids: Science and Technology, Wiley Interscience, New Jersey, 2007.

[3] Mahmoodi M., Kandelousi S., Cooling process ofLiquid Propellant Rocket by Means of Kerosene-Alumina Nanofluid. *Propulsion and Power Research*, (2016). http://dx.doi.org/10.1016/j.jppr.2016.11.003

[4] Das, K. Sarkar, A. Kundu, P. K. Nanofluid Flow over a Stretching Surface in Presence of Chemical Reaction and Thermal Radiation: An Application of Lie Group Transformation. *Journal of Siberian Federal University. Mathematics & Physics*, vol. 10, issue 2, pp. 146-157, (2017).

[5] Ellahi, R. The Effects of MHD and Temperature Dependent Viscosity on the Flow of non-Newtonian Nanofluid in a Pipe: Analytical Solutions. *Appl. Math. Model*, vol. 37, issue 3, pp. 1451-1467, (2013).

[6] Liu, J. T. C. Fuller, M. E. Wu, K. L. Czulak, A. Kithes, A. G. Felten, C. J. NanofluidFlow and Heat Transfer in Boundary Layers at Small Nanoparticle Volume Fraction: Zero Nanoparticle Flux at Solid Wall. *Arch. Mech.*, vol. 69, issue 1, pp. 75-100, (2017).

[7] Sheikholeslami, M. Gorji-Bandpy, M. Ganji, D.D. Soleimani, S. Thermal Management for Free Convection of Nanofluid using Two Phase Model. *J. Mol. Liq.* , vol. 194, pp. 179-187, (2014).

[8] Malvandi, A. Hedayati, F. Ganji, D. D. Fluid Flow and Heat Transfer of Nanofluids over a Flat Plate with Conjugate Heat Transfer. *Trans. Phenom. Nano Micro Scales.* vol. 2, issue 2, pp. 108-117, (2014).

[9] Hatami, M. Sheikholeslami, M. Hosseini, M. Ganji, D.D. Analytical Investigation of MHD Nanofluid Flow in Nonparallel Walls. *J. Mol. Liq.* vol. 194, pp. 251-259, (2014).

[10] Hayat, T. Abbas, T. Ayub, M. Farooq, M. Alsaedi, A. Flow of Nanofluid Due to Convectively Heated Riga Plate with Variable Thickness. *Journal of Molecular Liquids*, vol. 222, pp. 854-862, (2016).

[11] Hatami, M. Sheikholeslami, M. Ganji, D.D. Nanofluid Flow and Heat Transfer in an Asymmetric Porous Channel with Expanding or Contracting Wall. *Journal of Molecular Liquids*, vol. 195, pp. 230-239, (2014).

[12] Sheikholeslami, M. KKL correlation for Simulation of Nanofluid Flow and Heat Transfer in a Permeable Channel. *Phys. Lett*, vol. Á378, issue 45, pp. 3331-3339, (2014).

[13] Sheikholeslami, M. Ganji, D.D. Nanofluid flow and heat transfer between parallel plates considering Brownian motion using DTM. *Comput. Methods Appl. Mech. Eng.* vol. 283, pp. 651-663, (2015).

[14] Domairry, D. Sheikholeslami, M. Ashorynejad, H.R. Subba, R. Gorla, R. Khani, M. Natural Convection Flow of a non-Newtonian Nanofluid between Two vertical Flat Plates. *Proc. IMechE Part N: J. Nanoeng. Nanosyst.* vol. 225, issue 3, pp. 115-122, (2012).

[15] He, J-H. Homotopy Perturbation Technique. *Comput.Methods Appl. Mech. Engrg.*, vol. 178, pp. 257-262, (1999).

[16] YaRudyak, V. Bord, E. G. On Stability of Plane and Cylindrical Poiseuille Flows of Nanofluids. *Journal of Applied Mechanics and Technical Physics*, vol. 58, pp. 1013-1020, (2017).

IJMAO

International Journal of Mathematical Analysis and Optimization: Theory and Applications
Vol. 2020, No. 1, pp. 669 - 688

[17] Adeniyan, A. Adigun, J. A. Stress-Work and Chemical Reaction Effects on MHD Forced Convection Heat and Mass Transfer Slip-Flow Towards a Convectively Heated Plate in a non-Darcian Porous Medium with Surface Mass Flux. *Int. J. of Mathematical Analysis and Optimization: Theory and Applications*, pp. 338-355, (2018).